FULL PAPERS

Magnetic Resonance in Medicine 46:31–38 (2001)

Differential Routing of Choline in Implanted Breast Cancer and Normal Organs

R. Katz-Brull, R. Margalit, and H. Degani*

Choline is an essential nutrient participating as the initial substrate in major metabolic pathways. The differential metabolic routing of choline was investigated in MCF7 human breast cancer implanted in nude mice and in the kidney, liver, and brain of these mice. The distribution of metabolites following infusion of [1,2-^{13}C]-choline was monitored by ^{13}C magnetic resonance spectroscopy. This infusion led to an 18-fold increase in plasma choline and to concomitant changes in the content and distribution of choline metabolites. In vivo kinetic studies of the tumor during the infusion demonstrated accumulation of choline in the interstitium and intracellular synthesis of phosphocholine. The amount of unlabeled choline metabolites was 7.1, 4.1, 3.5, and 1.4 μmol/g in the kidney, liver, tumor, and brain, respectively. The variations in the labeled metabolites were more pronounced with high amounts in the kidney and liver (8.0 and 4.3 μmol/g, respectively) and very low amounts in the tumor and brain (0.33 and 0.12 μmol/g, respectively). In the kidney and liver, betaine (unlabeled and labeled) was the predominant choline metabolite. The dominant unlabeled metabolite in breast cancer was phosphocholine and in the brain glycerophosphocholine. Magn Reson Med 46:31–38, 2001.

Key words: ^{13}C-MRS; liver; kidney; brain

Choline, a quaternary amine, is an essential nutrient for humans (1,2) and plays a critical role in brain development (3). The metabolism of choline is partitioned among three major pathways: 1) phosphorylation leading to the CDP-choline pathway (known also as the Kennedy pathway) for the synthesis of phosphatidylcholine (PtdCho); 2) acetylation to synthesize the neurotransmitter acetylcholine; 3) oxidation to produce the methyl donor betaine and S-adenosylmethionine (Fig. 1).

Following uptake of choline, it is first converted to phosphocholine (PCho) via the CDP-choline pathway, or to betaine through the oxidation pathway, or to acetylcholine, all water-soluble metabolites that can be present in appreciable amounts (mM range). Thus, the amount of these metabolites can be determined by choline transport and/or by the activities of the enzymes involved in their synthesis and further metabolism. Glycerophosphocholine (GPCho) is also a water-soluble, choline-derived metabolite; however, unlike the other metabolites described above, which are synthesized from choline in one or two steps, it is a breakdown product of PtdCho and therefore the regulation of its content is complex. The distribution of the water-soluble choline metabolites among the various pathways varies with tissue type and can be modulated by changing the choline intake via diet or direct infusion.

High levels of choline metabolites including PCho and GPCho were previously observed by ^{31}P and ^{1}H magnetic resonance spectroscopy (MRS) in various malignancies and specifically in breast cancer (4–11). The magnitude of the ^{1}H MRS signal of the trimethylamine moiety shared by choline and its derivatives was previously shown to aid in the diagnosis of breast cancer (5–7); however, it was not possible to resolve this signal. Previous studies monitored in vivo the uptake and metabolism of choline in mammary carcinoma using ^{31}P MRS to follow phosphonium-choline metabolism (12) and deuterium MRS to follow infused deuterium-labeled-choline (13).

MRS was also applied to investigate choline metabolism in normal organs (14,15). The content of the water-soluble choline metabolites in the brain was determined from the signal at 3.2 ppm of ^{1}H spectra. Although it was not possible to resolve this signal and identify the exact composition of the choline metabolites, its magnitude was indicative of brain tissue physiology and pathology, including brain tumors (4,16–19). The uptake and metabolism of choline in the brain and the kidney were also investigated in vivo by ^{13}C and ^{2}H MRS, respectively, utilizing labeling of the trimethylamine moiety of choline (14,15). In these studies, as in ^{1}H-MRS, the choline signal was not resolved but kinetic data were obtained.

Here we present comparative studies of choline metabolism in tumors of MCF7 human breast cancer implanted in nude mice and in the kidney, liver, and brain of these mice. The composition of the various choline metabolites was investigated by ^{13}C MRS following the signals of carbon 1 and 2 of choline at natural abundance and after infusion of enriched [1,2-^{13}C]-choline (20). The kinetics of choline uptake and metabolism in the tumors was also monitored in vivo. The results describe the specific differential routing of choline in each tissue.

MATERIALS AND METHODS

Animals

CD-1 athymic female mice, 6–8 weeks old (Weizmann Institute Animal Services) were housed in a controlled environment (24°C and daily cycles of 12 hr light/dark) and fed a semisynthetic diet of 50% corn supplemented with minerals, vitamins, 0.2% choline chloride, and 0.2% methionine. Food and water were supplied ad libitum.

Department of Biological Regulation, Weizmann Institute of Science, Rehovot, Israel.

Grant sponsor: Sir David Alliance, CBE, UK.

*Correspondence to: Prof. Hadassa Degani, Department of Biological Regulation, Weizmann Institute of Science, Rehovot, 76100, Israel.

Received 10 August 2000; revised 9 January 2001; accepted 9 January 2001.

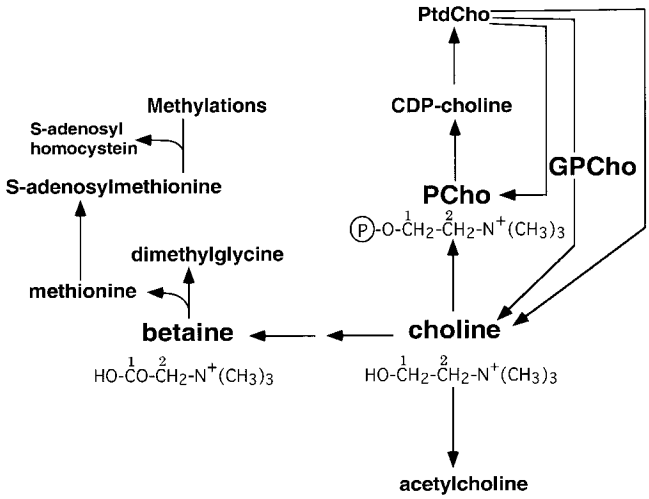

FIG. 1. Choline metabolism in mammalian cells: the Kennedy pathway, through CDP-choline, the oxidative pathway to betaine, and the acetylation pathway to acetylcholine. Positions marked 1 and 2 were labeled with carbon-13 ([1,2-^{13}C]-choline). PCho, phosphocholine; GPCho, glycerophosphocholine; PtdCho, phosphatidylcholine.

Tumors

MCF7 cells, cultured routinely as previously described (13), were inoculated s.c. ($\sim 10^7$ cells/mouse) in the right flank of CD-1 female athymic mice. Before the cell inoculation a pellet of 17β-estradiol (0.72 mg/pellet, 60 days release time; Innovative Research of America, Sarasota, FL) was implanted underneath the skin (21). Tumors were developed within 4–6 weeks to a size of ~ 3 cm^3. Choline infusion studies were performed on mice bearing these tumors.

Choline Infusion

The mice were anesthetized with pentobarbitone sodium (0.06 mg/g) injected i.p. with additional doses (0.014 mg/g) administered s.c. every 2 hr. Fifteen minutes prior to initiation of choline infusion, atropine (0.2 mg/Kg free base was injected into the tail vein. Then a sterilized solution (1 ml) of 50 mM [1,2-^{13}C]-choline chloride (99% enriched CIL; Cambridge Isotopes Laboratories, Andover, MA) and 100 mM sodium chloride was infused to the mice through the tail vein at a dose of 16 μmol/Kg/min.

Collection and Processing of Blood and Tissue Samples

Two hours after initiation of [1,2-^{13}C]-choline infusion, while the animals were under anesthesia and the infusion still on, blood and tissue samples were obtained in the following order: first heparinized blood (400 μl) was obtained by a retro orbital sinus puncture, then the tumor, kidneys, and liver were resected, and finally the animal was sacrificed by removing the brain. Each tissue sample was immediately immersed in liquid nitrogen. The whole process took about 1 min for each mouse. The tissue samples were moved for storage to −80°C until extraction. Tissue weight was measured before the extraction.

The blood was centrifuged for 10 min (at 1000 rpm) and D_2O (99.9% enriched CIL) was then added to the supernatant (plasma) to a total volume of 500 μl. The plasma samples were kept at −20°C. NMR measurements of these samples were performed in 5 mm tubes containing 5 μl of methanol as a standard for concentration.

Tissue Extracts

Extraction of the water-soluble metabolites and of the lipids was performed by the dual phase extraction (DPE) method following a procedure described previously for cell extracts (22), with slight modifications. Tissue samples were placed in 10 ml of ice-cold methanol containing 0.4 mM phenylphosphonic acid (Aldrich, Milwaukee, WI) for 1 hr. The tissue was then homogenized in the methanol solution within 20 sec. An equal volume of chloroform was added to the homogenate and the mixture was vigorously vortexed. Then 10 ml of double-distilled water were added and the mixture was vigorously vortexed again. This mixture was centrifuged at 1000 rpm until phase separation (~20 min). The upper methanol-water phase and the lower chloroform phase were separated. The methanol-water phase was treated with Chelex 100 (Sigma, St. Louis, MO), the mixture was vortexed, and the resin was separated by centrifugation. The supernatant was lyophilized to dryness and kept at −20°C. Before NMR measurement, the dried residue was redissolved in 0.5 ml 99.9% enriched D_2O containing 5 μl of methanol as a standard for ^{13}C measurements at pH of 8–8.3. Prior to the ^{31}P NMR studies, 10 mM EDTA (Fluka, Buchs, Switzerland) was added to minimize the interaction of the phosphate with the divalent ions. The chloroform phase was evaporated and the dried residue was redissolved in a mixture of 0.4 ml chloroform and 0.2 ml of methanolic EDTA (22). NMR measurements of both the water and lipid extracts were performed in 5 mm NMR tubes. Each sample of tumor, kidney, and liver contained an extract of a single specimen. For the brain, a combined extract from six mice was used to achieve detectable levels of metabolites.

NMR Spectroscopy of Plasma and Extract Samples

High-resolution NMR spectra were recorded on a DMX-500 spectrometer operating at 11.7 T (Bruker, Germany). ^{13}C spectra were recorded at 125.7 MHz using a ^{1}H/^{13}C dual probe and applying 60° pulses, 2.4 sec repetition time, and continuous composite pulse proton decoupling. The signal of added methanol (at 49.75 ppm) served as a concentration standard. ^{31}P NMR spectra were recorded at 202.4 MHz using a broadband probe by applying 45° pulses, repetition time of 2 sec, and continuous composite pulse proton decoupling. The chemical shifts were assigned in reference to α-ATP at −10.03 ppm. The signal of added phenylphosphonic acid served as a concentration standard.

In Vivo NMR Spectroscopy and MRI

In vivo studies were performed on a 4.7 T Biospec spectrometer (Bruker, Germany). ^{13}C spectra were recorded at 50.4 MHz using a home-built two-turn, 1-cm diameter ^{13}C surface coil placed within a 7.5-cm ^{1}H volume coil

(Bruker, Germany) by applying 90° adiabatic pulses, 2.4 sec repetition time, and composite pulse proton decoupling in a bilevel mode. The implanted tumor was placed on top of the surface coil, thus detecting signals arising predominantly from approximately 1 cm^3 of the tumor tissue (determined from the response profile of the probe). The signal of the natural abundance carbons of double bonds (at 130 ppm) served as an internal concentration standard. An external standard for concentration determination consisted of 5.4 μmol [1-^{13}C]-glucose (99% enriched, CIL) in 180 μl of water in a sealed plastic bag (less than 2 mm thickness), of a size similar to the coil surface area placed between the surface of the probe and the tumor.

MR images were recorded using the ^{1}H volume coil described above. Multislice, spin echo T_2-weighted images were recorded with an echo time of 80 ms, a repetition time of 3200 ms, slice thickness of 1 mm, in-plane resolution of 0.23 × 0.46 mm, and slice-to-slice distance of 0.2 mm. Total tumor volume was determined from the area and the thickness of each slice, and the slice-to-slice distance as previously described (21). The fraction of necrosis was measured by analyzing the intensity distribution in the T_2-weighted images as previously described (21). In each image several ROIs of viable regions (confirmed also by histology) were selected and the mean intensity of pixels in these regions was calculated. The number of pixels exhibiting an intensity ≥1.2-fold higher than this mean intensity divided by the total number of tumor pixels provided an estimate of the fraction of necrosis. At the end of the choline infusion and MR recordings the tumors were resected and processed for histology as previously described (21).

Data Analysis

Signal intensity and area in NMR spectra were measured with Bruker software XWIN-NMR. The areas were converted to concentration units taking into account enrichment, saturation, and nuclear Overhauser effect differences. The results for tumor, kidney, and liver are presented as the mean concentration ± SEM and for the brain as the mean concentration ± integration error.

The changes with time in the [1,2-^{13}C]-choline concentration in the tumor (C_{tumor}) were analyzed assuming that choline diffusion transfer rate from the intravascular to the extracellular tumor compartment and choline transport rate (V_{trans}) into the intracellular compartment determine the observed choline kinetics. The rate of change in the concentration of [1,2-^{13}C]-choline in the tumor during the infusion time is therefore:

$$dC_{tumor}/dt = (k/\upsilon)(C_p - C_{tumor}) - V_{trans}. \quad [1]$$

Where k is the diffusion transfer constant, υ is the average extracellular volume fraction ($0 \le \upsilon \le 1$), and C_p is the plasma [1,2-^{13}C]-choline concentration, assumed to be constant during the infusion, as previously shown (13,23). V_{trans} was estimated from the linear increase in the signal of labeled PCho (average of n = 6) which represented PCho synthesis rate. Choline transport was previously shown to be the rate limiting step in PCho synthesis in MCF7 cells (24).

The solution of this equation for the initial condition $C_{tumor}(0) = 0$, is:

$$C_{tumor}(t) = (C_p - V_{trans}(k/\upsilon)^{-1})(1 - \exp(-t\,k/\upsilon)). \quad [2]$$

The experimental data were fitted to this equation using a nonlinear least-square program yielding k/υ.

RESULTS

The fate of [1,2-^{13}C]-choline infused through the blood circulation in nude mice was investigated in implanted MCF7 breast tumors and in the plasma, kidney, liver, and brain utilizing ^{13}C and ^{31}P MRS. It should be noted that prior to choline infusion the mice were treated with atropine in order to prevent the occurrence of overt cholinergic intoxication symptoms (25).

Studies of Plasma

The concentration of [1,2-^{13}C]-choline in the plasma after ~2 hr of continuos infusion was 1.00 ± 0.18 mM (n = 8). This level was markedly higher than the initial plasma concentration of choline in these mice of 0.058 ± 0.010 mM (13). Thus, the infusion led to about an 18-fold increase in the plasma choline pool, above the K_m of choline transport that spans a broad range between 1 to ~500 μM (26–28). [1,2-^{13}C]-Betaine in the plasma, derived from the [1,2-^{13}C]-choline, increased as well and reached a level of 0.14 ± 0.02 mM (n = 8).

Studies of Extracts of Tumors, Kidney, Liver, and Brain

The metabolic routing of choline in tumors and in normal organs was studied following 2 hr infusion of [1,2-^{13}C]-choline using ^{13}C and ^{31}P NMR of tissue extracts. High-resolution ^{13}C spectra of the water-soluble phase of these extracts (Fig. 2) showed signals due to free choline, betaine, and PCho at natural abundance and their 99% enriched [1,2-^{13}C]-counterparts. The observed GPCho signals were due solely to the natural abundant, nonlabeled metabolite. In the tumors (n = 8) the concentration of these metabolites at natural abundance followed the order: PCho > GPCho ≫ choline, with betaine below detection level (Table 1). The ratio of PCho to choline was high: 22 ± 2. After the infusion, significant amounts of [1,2-^{13}C]-PCho and -choline were detected (Table 2). The resultant ratio of [1,2-^{13}C]-PCho to [1,2-^{13}C]-choline (0.26 ± 0.06) was reversed relative to the ratio of the respective natural abundant pools; however, the ratio of the total pools (7.4 ± 0.7) still markedly favored PCho. [1,2-^{13}C]-Betaine was detected in the tumor at a low level (Table 2).

The total concentration of choline metabolites at ^{13}C natural abundance in the various organs was within the same order of magnitude as that of the tumor, with the highest content in the kidney and the lowest in the brain (Table 1). The distribution of the metabolites followed the order: kidney: GPCho ≈ betaine ≫ PCho ≥ choline; liver: betaine ≥ PCho ≫ GPCho ≥ choline; and brain: GPCho > PCho > choline, with betaine below the detection limit

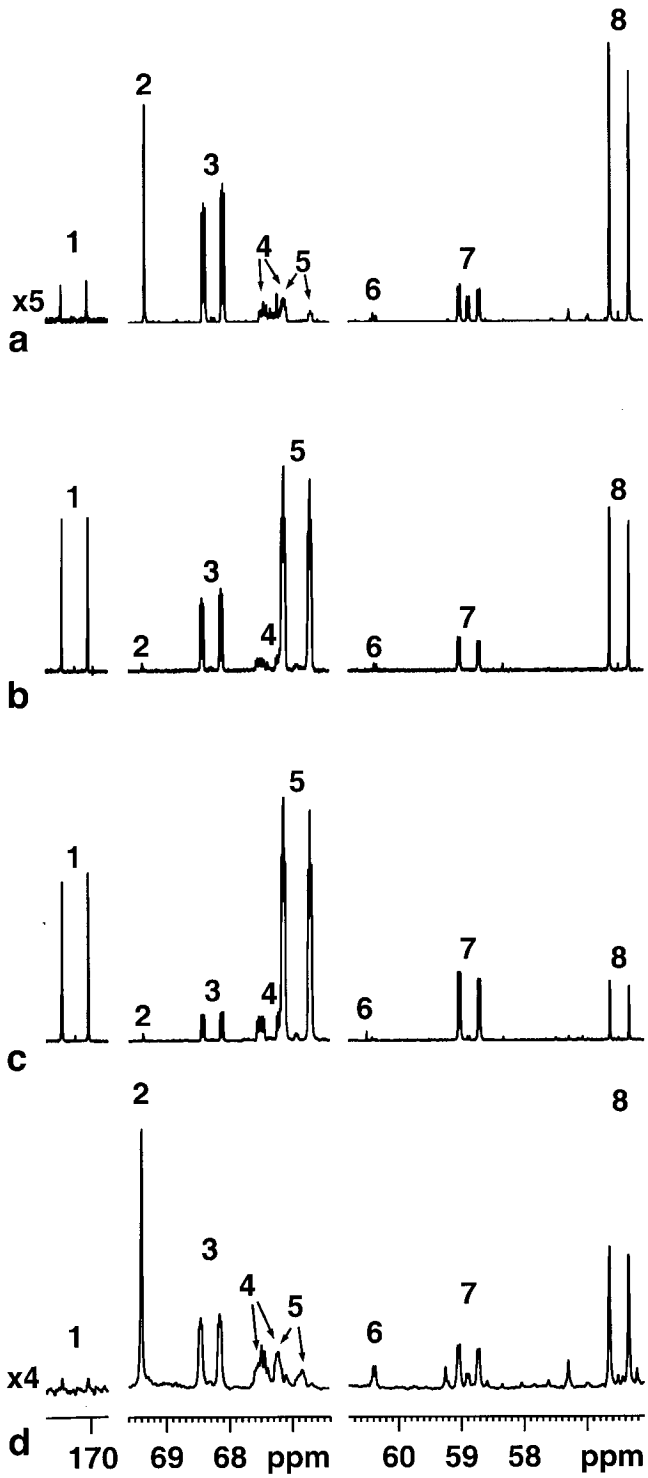

FIG. 2. ^{13}C spectra of the water-soluble phase of MCF7 tumor (**a**), kidney (**b**), liver (**c**), and brain (**d**) extracts after 2 hr of infusion with [1,2-^{13}C]-choline. The spectra were recorded as described in Materials and Methods by acquiring 65,600 (**a**), 9,600 (**b**), 8,000 (**c**), and 102,400 (**d**) scans for 5–68 hr and were processed with a line broadening of 0.1 Hz (**a–c**) and with gaussian multiplication (**d**). Assignment: 1) betaine-C_1, 2) lactate-C_2, 3) choline-C_2, 4) PCho-C_2, 5) betaine-C_2, 6) GPCho-C_1, 7) PCho-C_1, 8) choline-C_1. The positions C_1 and C_2 of choline, PCho, betaine, and GPCho are shown in Fig. 1.

(Table 1). After 2 hr infusion the concentration of labeled choline metabolites in the kidney and liver was more than one order of magnitude higher than that in the tumor and the brain (Table 2). The predominant labeled metabolite in the liver and kidney was [1,2-^{13}C]-betaine (Table 2). In the brain most of the label was in the form of free [1,2-^{13}C]-choline but [1,2-^{13}C]-PCho and -betaine were also observed (Table 2). Thus, both the composition of choline metabolites and the metabolic fate of newly incorporated choline were found to be tissue-specific. Clearly, MCF7 human breast tumors were distinctive in their high PCho content and low betaine content and demonstrated slow choline uptake (similar to the brain) relative to the kidney and liver.

The energy state of the tumors was determined and compared to the known physiology of the same cells in culture by recording ^{31}P spectra of the water-soluble tumor extracts. The total PCho pool in the tumors was 2.1 ± 0.2 μmol/g tissue (n = 8), confirming the results obtained from the ^{13}C spectra (Table 1). The NTP + NDP (nucleoside-tri- and -di-phosphate, respectively) concentration of the tumors was 0.86 ± 0.09 μmol/g tissue. As is the case in extracts, the presence of NDP is presumably due to phosphatase activity in the course of the extraction. The ratio of PCho to NTP + NDP was equal to 2.44 ± 0.17 (n = 8) and similar to the ratio of PCho to NTP of MCF7 cells in culture (29).

^{13}C and ^{31}P spectra of the lipid phase of the tumors did not show significant incorporation of ^{13}C label after 2 hr infusion into choline-derived phospholipids such as PtdCho and sphingomeylin. This is in accord with previous studies of breast cancer cells that demonstrated 36% incorporation in 24 hr (13).

In Vivo Uptake and Metabolism of Choline in Tumors

Choline metabolism in tumors was further investigated in vivo in the course of [1,2-^{13}C]-choline infusion. Analysis of the MRI data yielded an average tumor size ± SEM of 3.4 ± 0.4 cm^3 (n = 6), with a low fraction of necrosis ranging between 3–13%. The low fraction of necrosis was scattered within the tumor and not concentrated in central parts. Histological examination of the tumors confirmed the presence of a high fraction of viable tissue in these tumors.

An example of T_2-weighted images and histological sections of a tumor is shown in Fig. 3. The histological sections (Fig. 3, sections 7–9) were sliced at a plane similar to that of the MR images. The lower panel of this figure demonstrates selected viable and necrotic regions under large magnification. The gray regions in the T_2-weighted images (Fig. 3, images 1–6) demonstrate the presence of viable tumor tissue and the bright regions present necrosis (21). The fraction of necrosis in this tumor was found to be 11%.

^{13}C spectra of the tumors recorded in the course of [1,2-^{13}C]-choline infusion revealed a gradual increase in the intensity of the signals at the chemical shifts of choline and PCho, while the signals in the range of 20–40 and 124–134 ppm (due to methylene moieties and double bonds of fatty acyl chains, respectively (30)) remained unchanged (Fig. 4). The signals of [1,2-^{13}C]-PCho appeared

Table 1
Composition of Choline Metabolites Present at ^{13}C Natural Abundance

Tissue extracts	Total content μmol/g	Choline (%)[1]	PCho (%)[1]	GPC (%)[1]	Betaine (%)
MCF7 tumor (n = 8)	3.5 ± 0.3[a]	3.2 ± 0.6	75 ± 2[b,c]	22 ± 2[b,c]	Not detected
Kidneys (n = 5)	7.1 ± 2.4	2.9 ± 1.5	K-L[4] 6 ± 2[d]	48 ± 6[d]	43 ± 5
Liver (n = 5)	4.1 ± 1.8	1.8 ± 1.2	41 ± 6	5 ± 3	52 ± 6
Brain[2] (n = 6)	1.4 ± 0.3	12 ± 2	33 ± 7	56 ± 11	Not detected

[1]The relative concentration of each metabolite with respect to the total pool of choline metabolites. Results are presented as mean ± SEM.
[2]Obtained from a ^{13}C spectrum of a combined sample of extracts (see Materials and Methods).
[a]Significant difference (two-tail t-test $p < 0.05$) between tumor and kidneys.
[b,c]Highly significant difference ($p < 0.005$) between tumor and liver and tumor and kidney, respectively.
[d]Highly significant difference ($p < 0.005$) between kidney and liver.

after the first hour of infusion and increased linearly with time thereafter (Fig. 5a). The time course of this increase was similar in all the tumors, yielding an average initial rate of PCho synthesis of 0.12 ± 0.04 mM/h (n = 6). The signals of [1,2-^{13}C]-choline increased as well (Fig. 5b) and the time course of this increase was analyzed according to Eq. [2] (Fig. 5b), assuming that most of the choline is in the extracellular volume. The ratio: choline diffusion transfer constant / extracellular volume fraction (k/υ) was 0.36 ± 0.08 h^{-1} (n = 6).

Upon termination of the infusion the intensities of [1,2-^{13}C]-choline signals decreased to basal level within 2 hr (Fig. 5b), while those of [1,2-^{13}C]-PCho remained unchanged (Fig. 5a). This decrease paralleled the reduction in plasma [1,2-^{13}C]-choline (13,31), confirming the predominant presence of [1,2-^{13}C]-choline in the extracellular volume during the infusion.

DISCUSSION

The total pool of choline and choline-derived metabolites has been previously followed in vivo by MRS through the ^{1}H signal of the trimethylamine group (5–7,16–19). Uptake and metabolism of choline was also previously monitored in vivo by following ^{2}H- and ^{13}C-choline enriched at the trimethylamine group (13–15). However, in these studies the overlapping signal could not be resolved to the various choline metabolites and therefore changes in this signal could not be interpreted in terms of the associated metabolic processes. Here we used a different labeling strategy in which the two methylene carbons of choline were labeled with ^{13}C. The signals of these carbons are separated by 12 ppm (in choline) and are split by ^{13}C–^{13}C J-coupling. The carbon in position 2 is further split by the interaction with ^{14}N. The chemical shift of the carbon in position 1 is extremely sensitive to the functional group attached to it: for choline 56.5 ppm, PCho 58.9 ppm, GPCho 60.3 ppm, and betaine 170.2 ppm. Thus, the distinct chemical shift and coupling properties made it possible to resolve and assign the choline metabolites in extracts and in vivo. The characteristic ^{13}C–^{13}C splitting also enabled us to differentiate between ^{13}C-labeled and nonlabeled molecules.

Labeling in vivo required administration of ^{13}C-choline into the blood circulation. It was previously shown that the half-life of choline in the blood is very short (<1 min) due to fast clearance by the kidney and the liver (31,32).

Table 2
Composition of [1,2-^{13}C]-Choline Metabolites After 2 h of [1,2-^{13}C]-Choline Infusion

Tissue extracts	Content of [1,2-^{13}C]-labeled metabolites μmol/g	[1,2-^{13}C]-choline (%)[1]	[1,2-^{13}C]-PCho (%)[1]	[1,2-^{13}C]-betaine (%)[1]	Total content of choline metabolites labeled + naturally abundant μmol/g	Enriched fraction of choline metabolites
MCF7 tumor (n = 8)	0.33 ± 0.05[a,b]	76 ± 4[a,b]	19 ± 3[b,c]	5 ± 1[a,b]	3.8 ± 0.3[b,c]	0.090 ± 0.014[a,b]
Kidneys (n = 5)	8.0 ± 1.2[d]	36 ± 7[e]	7 ± 1[e]	57 ± 7[e]	15 ± 3	0.57 ± 0.07
Liver (n = 5)	4.3 ± 1.8	10 ± 3	12 ± 2	78 ± 3	8.4 ± 2.6	0.56 ± 0.08
Brain[2] (n = 6)	0.12 ± 0.02	50 ± 10	27 ± 5	23 ± 5	1.5 ± 0.3	0.079 ± 0.016

[1]The relative concentration of each [1,2-^{13}C]-choline metabolite with respect to the total pool of [1,2-^{13}C]-choline metabolites. Results are presented as mean ± SEM.
[2]Obtained from a ^{13}C spectrum of a combined sample of extracts (see Materials and Methods).
[a,b]Highly significant difference (two-tail t-test $p < 0.005$) between tumor and liver and tumor and kidney, respectively.
[c]Significant difference ($p < 0.05$) between tumor and liver.
[d]Significant difference ($p < 0.05$) between kidney and liver.
[e]Highly significant difference ($p < 0.005$) between kidney and liver.

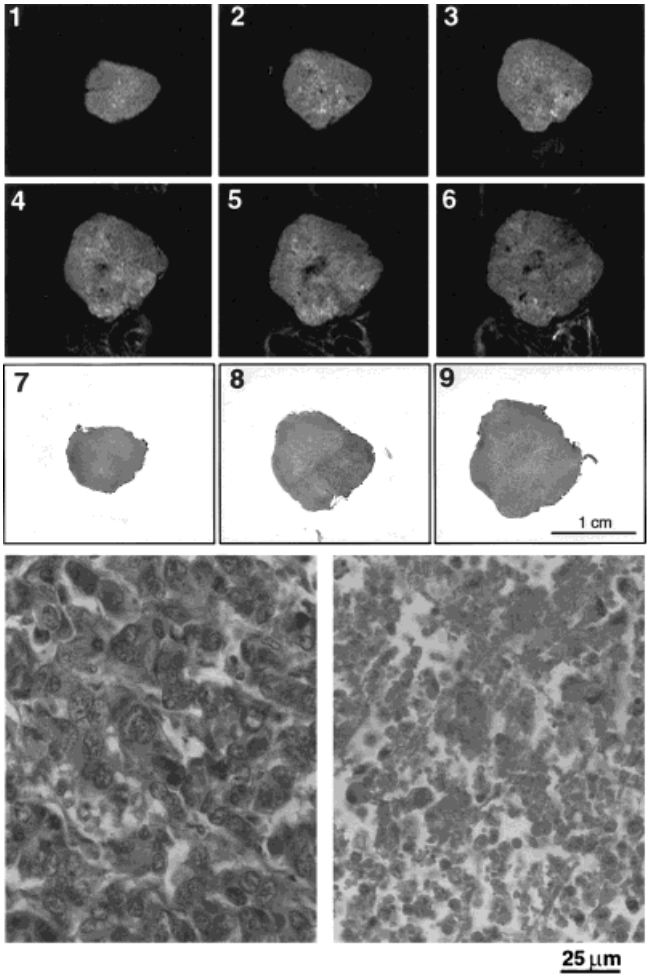

FIG. 3. MR images and histological sections of MCF7 tumor. MR images 1–6 show viable areas in gray and dark fibrous tissue as well as necrotic areas, which appear bright. Hematoxylin-eosin-stained histological sections (7–9) were sliced at a plane similar to that of the MR images (1, 3, 6, respectively). The lower panel demonstrates viable (left) and necrotic (right) regions at high magnification. This tumor was also investigated by in vivo ^{13}C MRS.

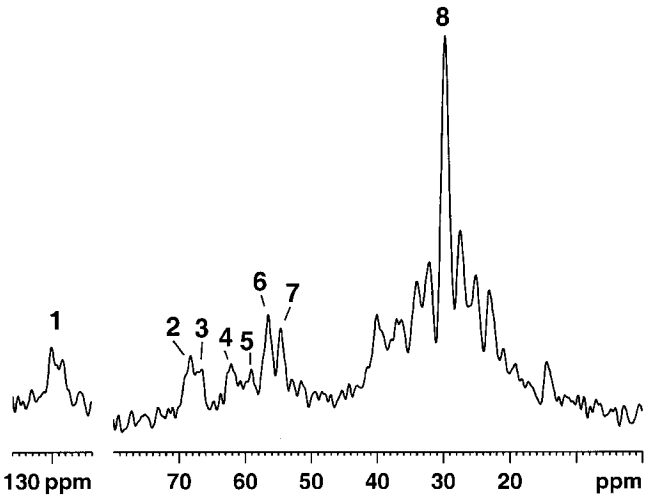

FIG. 4. ^{13}C spectrum of MCF7 tumor recorded in vivo during infusion of [1,2-^{13}C]-choline (at 4 h of infusion). The spectrum was acquired within 40 min (1000 scans) and processed with a gaussian multiplication. Assignment: 1) fatty acyl chain C=C at natural abundance (NA); 2) choline-C_2; 3) PCho-C_2, betaine-C_2, and glycerol (ester)-C_2 (NA); 4) glycerol (ester)-C_1 and -C_3 (NA); 5) PCho-C_1; 6) choline-C_1; 7) choline metabolites-$(CH_3)_3$ (NA); 8) fatty acyl chain -CH_2- (NA).

Therefore, to achieve a prolonged and constant high level of blood choline it was necessary here to perform a continuous infusion (23,31). After the infusion, the amount of choline metabolites in the kidney and liver increased by more than 2-fold and the predominant metabolite (labeled + unlabeled) in both organs was betaine. The fast and substantial synthesis of new labeled betaine indicated activation of betaine synthesis in addition to the fast transfer of the choline from the blood and the transport of choline to the cells and then into the mitochondria, the site of betaine synthesis. The substantial accumulation of betaine in both the liver and kidney appears to serve as a regulation mechanism for high choline. On the other hand, in the brain, despite the high blood levels, uptake and metabolism of labeled choline were lowest and the distribution of the total pools of choline metabolites remained similar, indicating protection from excess choline by the blood–brain barrier, as previously shown (32,33).

The high levels of betaine and also of GPCho observed in the current study in the kidney are also associated with their role as renal osmolytes (34). However, high GPCho levels were detected only in the unlabeled form, presumably as a result of slow incorporation of label into PtdCho, the precursor of GPCho. High levels of unlabeled GPCho were also found in the current study in the brain, in accord with previous findings in guinea pig brain (35). In general, GPCho levels are regulated by the activities of phospholipase A enzymes and GPCho:choline phosphodiesterase. The choline signal previously exhibited in ^1H spectra of the brain may therefore reflect the predominant presence of GPCho and presumably the differential activities of these two enzymes. The role of GPCho in the brain is not known, but Alzheimer's disease was found to be associated with increased GPCho and decreased choline levels (36). Clearly, in order to verify these changes by MRS it is necessary to resolve the choline signal to its components. Interestingly, despite the low incorporation of labeled choline we detected betaine synthesis in amounts similar to

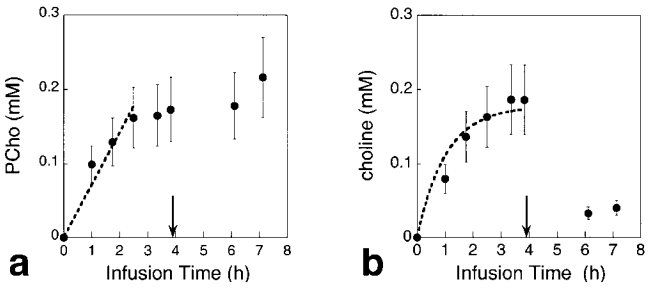

FIG. 5. Accumulation of [1,2-^{13}C]-PCho (**a**) and [1,2-^{13}C]-choline (**b**) in MCF7 tumor implanted in nude female mouse infused with [1,2-^{13}C]-choline. The arrow indicates termination of infusion. The dashed line represents a linear fitting in **a** and a fitting to Eq. [2] in **b**. The fitting yielded a slope of 0.05 mM/h (**a**) and k/υ of 0.18 h^{-1} (**b**).

PCho synthesis; however, the role of betaine in the brain is not clear.

The high level of unlabeled PCho observed here in the tumors of breast cancer was distinct. This metabolite was also the predominant intracellular labeled product. Small amounts of labeled betaine were also detected in the tumors, as previously demonstrated using the phosphonium choline analog (12). High PCho levels were found previously in the same cells in culture, as well as in other breast cancer cell lines. On the other hand, very low levels of this metabolite were found in normal human mammary epithelial cells (29,37,38). The metabolic changes that may lead to the accumulation of PCho as a result of malignant transformation are: 1) increase of choline kinase activity (39); 2) increase in choline transport activity (24); 3) decrease in CTP:phosphocholine cytidylyltransferase activity (39, and references therein); 4) activation of phospholipases and enhanced breakdown of GPCho (10). Studies in MCF7 cells and transformed cells have indicated that the first two alternatives predominate (24,39, and references therein).

During the infusion, labeled choline was augmented in the tumor, surpassing the level of labeled PCho. This reflected accumulation of choline either in the interstitial space or in the intracellular space or both. Based on previous studies which indicated very low intracellular choline in the same cells (24), it was assumed that most of the choline is confined to the interstitial space. The fast decrease in labeled choline after termination of the infusion lends support to this assumption. The kinetic behavior of choline in the extracellular volume was analyzed according to Eq. [2]. This equation is valid for time points in which $C_{\text{tumor}} > K_m$ (the concentration of choline in the tumor and the K_m for choline transport into the tumor cells). Already at the first experimental time point (during 40 min of infusion) C_{tumor} was mostly above K_m (K_m = 46 μM (24)). Therefore, Eq. [2] was valid for analyzing the kinetic behavior. Assuming an average extracellular volume fraction of about 0.5 (40), the kinetic analysis yielded a transfer constant of about 0.2 h^{-1}. This transfer constant provides an estimation of the permeability of the blood vessels to choline from which the time necessary to reach choline equilibration can be calculated ($1/k$). This permeability assessment may be unique to the tumor vasculature. The amount of choline in the tumor reached the high blood level concentration after about 4–5 hr (see Fig. 5), reconfirming the predominant presence of choline in the interstitium. Unlike in the kidney and liver, the transport of choline from the interstitial spaces into the tumor cells appeared to be rate-limiting and therefore the distribution of the choline metabolites was not markedly affected by the large increase in blood choline. Based on these results, we propose that the intensity of the ^{1}H choline signal in breast cancer patients reflects the predominant presence of PCho. Furthermore, we predict that increased concentration of blood choline by transient infusion to the blood circulation would not markedly change PCho content; however, choline may accumulate in the interstitium.

In summary, we have demonstrated the importance of resolving the choline signal components and the use of ^{13}C MRS and of [1,2-^{13}C]-choline in the investigation of the specific bifurcation of choline metabolism in normal and diseased tissues.

ACKNOWLEDGMENTS

We thank Prof. M. Liscovitch and Dr. P. Bendel from the Weizmann Institute and Prof. M. Cohn from the University of Pennsylvania for their help and support in the course of this study. H.D. is the incumbent of the Fred and Andrea Fallek Professorial Chair for Breast Cancer Research.

REFERENCES

1. Blusztajn JK. Choline, a vital amine. Science 1998;281:794–795.
2. Zeisel SH. Choline. A nutrient that is involved in the regulation of cell proliferation, cell death, and cell transformation. Adv Exp Med Biol 1996;399:131–141.
3. Cermak JM, Holler T, Jackson DA, Blusztajn JK. Prenatal availability of choline modifies development of the hippocampal cholinergic system. FASEB J 1998;12:349–357.
4. Negendank W. Studies of human tumors by MRS: a review. NMR Biomed 1992;5:303–324.
5. Roebuck JR, Cecil KM, Schnall MD, Lenkinski RE. Human breast lesions: characterization with proton MR spectroscopy. Radiology 1998;209:269–275.
6. Gribbestad IS, Singstad TE, Nilsen G, Fjosne HE, Engan T, Haugen OA, Rinck PA. In vivo ^{1}H MRS of normal breast and breast tumors using a dedicated double breast coil. J Magn Reson Imag 1998;8: 1191–1197.
7. Mackinnon WB, Barry PA, Malycha PL, Gillett DJ, Russell P, Lean CL, Doran ST, Barraclough BH, Bilous M, Mountford CE. Fine-needle biopsy specimens of benign breast lesions distinguished from invasive cancer ex vivo with proton MR spectroscopy. Radiology 1997;204:661–666.
8. Sijens PE, Wijredeman HK, Moerland MA, Bakker GJG, Vermeulen JWA, Luyten RR. Human breast cancer in vivo: H-1 and P-31 MR spectroscopy at 1.5 T. Radiology 1988;169:615–620.
9. Degani H, Horowitz A, Itzchak Y. Breast tumors: evaluation with P-31 MR spectroscopy. Radiology 1986;161:53–55.
10. Podo F. Tumor phospholipid metabolism. NMR Biomed 1999;12:413–439.
11. Leach MO, Verrill M, Glaholm J, Smith TA, Collins DJ, Payne GS, Sharp JC, Ronen SM, McCready VR, Powles TJ, Smith IE. Measurements of human breast cancer using magnetic resonance spectroscopy: a review of clinical measurements and a report of localized ^{31}P measurements of response to treatment. NMR Biomed 1998;11:314–340.
12. Street JC, Szwergold BS, Matei C, Kappler F, Mahmood U, Brown TR, Koutcher JA. Study of the metabolism of choline and phosphatidylcholine in tumors in vivo using phosphonium-choline. Magn Reson Med 1997;38:769–775.
13. Katz-Brull R, Bendel P, Margalit R, Degani H. Choline metabolism in breast cancer; ^{2}H, ^{13}C and ^{31}P NMR studies of cells and tumors. MAGMA 1998;6:44–52.
14. Eng J, Berkowitz BA, Balaban RS. Renal distribution and metabolism of [$^2H_9$] choline. A ^{2}H NMR and MRI study. NMR Biomed 1990;3:173–177.
15. Tunggal B, Hofmann K, Stoffel W. In vivo ^{13}C nuclear magnetic resonance investigations of choline metabolism in rabbit brain. Magn Reson Med 1990;13:90–102.
16. Preul MC, Caramanos Z, Collins DL, Villemure JG, Leblanc R, Olivier A, Pokrupa R, Arnold DL. Accurate, noninvasive diagnosis of human brain tumors by using proton magnetic resonance spectroscopy. Nat Med 1996;2:323–325.
17. Cohen BM, Renshaw PF, Stoll AL, Wurtman RJ, Yurgelun-Todd D, Babb SM. Decreased brain choline uptake in older adults. An in vivo proton magnetic resonance spectroscopy study. JAMA 1995;274:902–907.
18. Bitsch A, Bruhn H, Vougioukas V, Stringaris A, Lassmann H, Frahm J, Bruck W. Inflammatory CNS demyelination: histopathologic correlation with in vivo quantitative proton MR spectroscopy. Am J Neuroradiol 1999;20:1619–1627.

19. Gupta RK, Sinha U, Cloughesy TF, Alger JR. Inverse correlation between choline magnetic resonance spectroscopy signal intensity and the apparent diffusion coefficient in human glioma. Magn Reson Med 1999;41:2–7.
20. Ronen SM, Degani H. The application of ^{13}C NMR to the characterization of phospholipid metabolism in cells. Magn Reson Med 1992;25: 384–389.
21. Furman-Haran E, Maretzek AF, Goldberg I, Horowitz A, Degani H. Tamoxifen enhances cell death in implanted MCF7 breast cancer by inhibiting endothelium growth. Cancer Res 1994;54:5511–5514.
22. Tyagi RK, Azrad A, Degani H, Salomon Y. Simultaneous extraction of cellular lipids and water-soluble metabolites: evaluation by NMR spectroscopy. Magn Reson Med 1996;35:194–200.
23. Freeman JJ, Choi RL, Jenden DJ. Plasma choline: its turn over and exchange with brain choline. J Neurochem 1975;24:729–734.
24. Katz-Brull R, Degani H. Kinetics of choline transport and phosphorylation in human breast cancer cells; NMR application of the zero trans method. Anticancer Res 1996;16:1375–1380.
25. Agut J, Font E, Sacristan A, Ortiz JA. Dissimilar effects in acute toxicity studies of CDP-choline and choline. Arzne Forsch 1983;33:1016–1018.
26. Xin Q, Wightman RM. Transport of choline in rat brain slices. Brain Res 1997;776:126–132.
27. Porter RK, Scott JM, Brand MD. Choline transport into rat liver mitochondria. Characterization and kinetics of a specific transporter. J Biol Chem 1992;267:14637–14646.
28. Grunewald RW, Oppermann M, Muller GA. Choline transport and its osmotic regulation in renal cells derived from the rabbit outer medullary thick ascending limb of Henle. Pflugers Arch Eur J Physiol 1997; 434:815–821.
29. Ting YT, Sherr D, Degani H. Variations in the energy and phospholipid metabolism in normal and cancer human mammary epithelial cells. Anticancer Res 1996;16:1381–1388.
30. Canioni P, Alger JR, Shulman RG. Natural abundance Carbon-13 nuclear magnetic resonance spectroscopy of liver and adipose tissue of the living rat. Biochemistry 1983;22:4974–4980.
31. Choi RL, Freeman JJ, Jenden DJ. Kinetics of plasma choline in relation to turnover of brain choline and formation of acetyl choline. J Neurochem 1975;24:735–741.
32. Gardiner JE, Gwee MCE. The distribution in the rabbit of choline administered by injection or infusion. J Physiol Lond 1974;239:459–476.
33. Haubrich DR, Wang PF, Wedeking PW. Distribution and metabolism of intravenously administered choline[methyl- 3-H] and synthesis in vivo of acetylcholine in various tissues of guinea pigs. J Pharmacol Exp Ther 1975;193:246–255.
34. Burg MB. Molecular basis of osmotic regulation. Am J Physiol 1995; 268:F983–996.
35. Glonek T, Kopp SJ, Kot E, Pettegrew JW, Harrison WH, Cohen MM. P-31 nuclear magnetic resonance analysis of brain: the perchloric acid extract spectrum. J Neurochem 1982;39:1210–1219.
36. Wurtman RJ. Choline metabolism as a basis for the selective vulnerability of cholinergic neurons. Trends Neurosci 1992;15:117–122.
37. Aboagye EO, Bhujwalla ZM. Malignant transformation alters membrane choline phospholipid metabolism of human mammary epithelial cells. Cancer Res 1999;59:80–84.
38. Singer S, Souza K, Thilly WG. Pyruvate utilization, phosphocholine and adenosine triphosphate (ATP) are markers of human breast tumor progression: a ^{31}P and ^{13}C-nuclear magnetic resonance (NMR) spectroscopy study. Cancer Res 1995;55:5140–5145.
39. Ishidate K. Choline/ethanolamine kinase from mammalian tissues. Biochim Biophys Acta 1997;1348:70–78.
40. Furman-Haran E, Grobgeld D, Degani H. Dynamic contrast-enhanced imaging and analysis at high spatial resolution of MCF7 human breast tumors. J Magn Reson 1997;128:161–171.